Title
INCOMPLETE AND COMPLETE FUSION IN INTERMEDIATE ENERGY HEAVY ION REACTIONS

Author
Aleklett, K.

Publication Date
1986-06-01

LBL-21811
Preprint

Lawrence Berkeley Laboratory
UNIVERSITY OF CALIFORNIA

Submitted to Physica Scripta

INCOMPLETE AND COMPLETE FUSION IN INTERMEDIATE ENERGY HEAVY ION REACTIONS

K. Aleklett, W. Loveland, T.T. Sugihara, A.N. Behkami, D.J. Morrissey, L. Wenxin, W. Kot, and G.T. Seaborg

June 1986

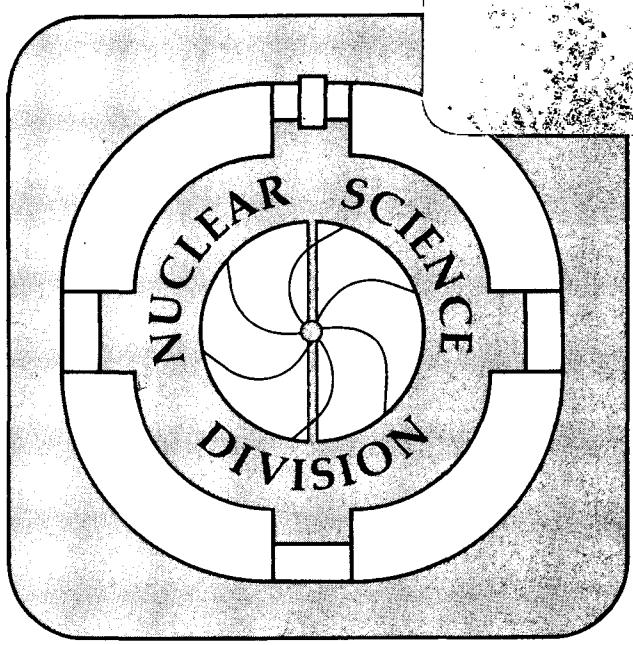

Prepared for the U.S. Department of Energy under Contract DE-AC03-76SF00098

DISCLAIMER

Incomplete and Complete Fusion in Intermediate Energy Heavy Ion Reactions

K. Aleklett
Studsvik Science Research Laboratory
S-611 82 Nykoping, Sweden

W. Loveland, T. T. Sugihara, and A. N. Behkami
Oregon State University, Corvallis, OR 97331, USA

D.J. Morrissey
Michigan State University, MI 48824, USA

Li Wenxin, Wing Kot and G.T. Seaborg
Lawrence Berkeley Laboratory, University of California
Berkeley, CA 94720, USA

This work was supported by the Director, Office of Energy Research, Division of Nuclear Physics of the Office of High Energy and Nuclear Physics of the U.S. Department of Energy under Contract No. DE AC03-76SF00098.

Incomplete and Complete Fusion in Intermediate Energy Heavy Ion Reactions

K. Aleklett
Studsvik Science Research Laboratory
S-611 82 Nykoping, Sweden

W. Loveland, T.T. Sugihara, and A. N. Behkami
Oregon State University, Corvallis, OR 97331, USA

D.J. Morrissey
Michigan State University, MI 48824, USA

Li Wenxin, Wing Kot and G.T. Seaborg
Lawrence Berkeley Labortory, Berkeley, CA 94720, USA

Abstract

The yields, angular distributions and differential range spectra have been measured for individual target residues from the interaction of 8.5 MeV/A ^{16}O, 19 MeV/A ^{16}O, 35 MeV/A ^{12}C and 86 MeV/A ^{12}C with ^{154}Sm. From the measured data, fragment isobaric yields and velocity spectra were deduced. The results are compared to the predictions of a modified Boltzmann master equation model of precompound particle emission.

1. Introduction

In recent years, considerable interest has developed in characterizing nucleus-nucleus collisions in the intermediate energy regime (20-100 MeV/A). A number of studies have measured the average linear momentum transfer to the target nucleus in these collisions. The measurements have been summarized in a semiempirical relationship[1].

$$(P_{11}/P_{CN}) = -0.092\ \sqrt{E/A} + 1.273 \qquad (1)$$

The average fraction of the beam momentum transferred to the target nucleus decreases approximately linearly with increasing relative velocity of the colliding nuclei. As the projectile energy increases, incomplete fusion processes become increasingly important and it is worth noting that throughout this energy regime, the average fractional linear momentum transfer significantly exceeds that observed in relativistic nuclear collisions[2].

As informative as these measurements are, we felt that it would be useful to study the evolution of individual reaction channels rather than "average" behavior as a function of projectile energy for intermediate energy nucleus-nucleus collisions. In addition, we were intrigued by reports[3] of production of trans-target species with large probability (for $\Delta Z = +1$, $\sigma = 200 - 250$ mb) in the reaction of 86 MeV/A ^{12}C with lead and bismuth. Accordingly, we decided to begin a systematic study of the yields, angular distributions and velocity spectra (using differential range techniques) of target residues from the interaction of intermediate energy heavy ions with the n-rich rare earth targets ^{150}Nd, ^{154}Sm, and ^{176}Yb. Through the use of the n-rich rare earth targets we should severely repress the "masking effects" of the fission of any target residues or transfer products. In this paper we present a report of the data obtained for the interaction of intermediate energy heavy ions with ^{154}Sm.

2. Experimental

We have measured the yields, angular distribution and differential range spectra for target residues formed in the interaction of 8.5 MeV/A ^{16}O, 19 MeV/A ^{16}O, 35 MeV/A ^{12}C and 86 MeV/A ^{12}C with ^{154}Sm. The irradiations

with the 8.5 and 19 MeV/A ^{16}O were carried out at the LBL 88" cyclotron, while the irradiations with 35 MeV/A and 86 Mev/A ^{12}C were performed at the MSU superconducting cyclotron and the CERN SC synchrocylotron, respectively. Targets consisting of deposits of $^{154}Sm_2O_3$ (98.7% ^{154}Sm) of various thicknesses ranging from 0.3 to 1.0 mg/cm^2 on a 4.7 mg/cm^2 Be backing were irradiated for times of 3-7 hours with heavy ion beams ranging in intensity from 10^{10}-10^{12} ions/sec. In the differential range measurements, all fragments recoiling from the target in the forward hemisphere were stopped in a stack of Al foils of various thicknesses (0.25-1.6 mg/cm^2). In the angular distribution measurements, fragments emerging from the target were stopped in a cylindrical arrangement of catcher foils. Fragments emerging at 0-10° with respect to the incident beam were caught in a 35 mg/cm^2 C foil while fragments with $10° \leq \theta \leq 60°$ were caught in 17.6 mg/cm^2 mylar catchers.

Following irradiation, the catcher foils from the angular distribution measurements were cut into pieces representing various angular intervals. These pieces along with the individual foils from the differential range measurements and the target foils were assayed by γ-ray spectroscopy beginning a few minutes after end of irradiation and continuing for periods of up to 3 months in laboratories at MSU and LBL. The identification of the activities present in each foil and the calculation of cross sections from these measured activities has been described previously[4]. The total activity found in the target and catcher foils was used in calculating the nuclidic production cross sections.

In the angular distribution experiments, the resolution of the experiments was decided primarily by the angular width of the catcher foils (the beam

spot size was < 4 mm^2). The alignment and centering of the beam was checked prior to the irradiation, during the irradiation and after the irradiation using radiography and on-line monitoring devices. No correction was made to the measured data for the finite angular resolution of the catcher foils because it was not felt to be critical for understanding the physics revealed by the data. The effect of the finite target thickness upon the measured angular distributions has been evaluated recently for a similar study[5]. Stopping of the fragments in the target or large angle scattering in the target can be excluded although there is probably some smearing of the angular distributions due to small angle scattering in the target.

Because of very strongly forward-peaked character of the angular distributions, the projected range distributions measured in the differential range experiments are, in fact, the true range distributions. Using the range-velocity relationships of Northcliffe and Schilling[6], the differential range distributions were converted to invariant velocity distributions. (These range-velocity relationships have been previously shown[7] to be accurate to a few percent for ions of the same Z, A and energy as encountered in this study). No attempts have been made at this stage of the data analysis to correct for the effects of range straggling upon the data.

3. Phenomenological Models

To help us understnd the significant features of the data, we have chosen to compare our data to the Boltzmann master equation model as developed by Blann[8] for use with intermediate energy heavy ion reactions. In this model, the methods of quantum statistical mechanics are used to follow the propagation of excitation energy through the target nucleus. The

target nucleus is assumed to be a two component Fermi gas with all states filled up to the Fermi level. Nucleons from the projectile are added to the target nucleus in states above the Fermi level. The relaxation of these initial configurations by internal nucleon-nucleon scattering or emission into the continuum is followed using a classical Boltzmann transport equation that has been appropriately modified to take into account quantum mechanical effects.

The basic Boltzmann transport equation has the form

$$\frac{d(n_i g_i)}{dt} = \sum_{j,k,l} \omega_{kl,ij} g_k n_k g_l n_l (1-n_j)(1-n_i) g_i g_j - \sum_{j,k,l} \omega_{ij,kl} g_i g_j n_j (1-n_k)(1-n_l) g_k g_l - n_i g_i \omega_{i,i'} g_{i'} + \frac{d}{dt}(n_i g_i)_{fus}, \quad (2)$$

where n_i is the average occupation number and g_i the number of single particle states per MeV in an energy interval 1 MeV wide measured from the bottom of the compound nucleus well. The $\omega_{ab,cd}$ are the transition probabilities for nucleons in initial states a and b to scatter into final states c and d; they are evaluated from free nucleon-nucleon scattering cross sections. Pauli blocking is simulated by the $(1-n_i)$ terms. The last term in equation (2) represents the time dependent injection of excitons into the fusing system. To actually perform these calculations we have used the computer code of Harp and Blann.[9]

Using this model, we have calculated the average fractional linear momentum transfer to the target nucleus, and the spectra of the pre-equilibrium neutrons and protons for each system studied in this work, the calculated values of the fractional linear momentum transfer are in good agreement with the systematics expressed by equation (1). To calculate the average

angular momentum of the excited target residue, $\bar{J}$, following the pre-equilibrium particle emission, we have used the simple semiclassical expression

$$\bar{J} = \frac{P_{11}}{P_{CN}} \cdot \ell_{crit} \qquad (3)$$

Values of ℓ_{crit} were taken from Ref. 10. The distribution of J values in the excited target residue was taken to be a 2J+1 distribution beginning at J=0 and extending to J_{max} with mean value $\bar{J}$. The distribution of excitation energy values in the excited residual nucleus P(E*) was computed using the calculated pre-equilibrium n and p kinetic energy spectra, the known binding energies and conservation of energy.

We assumed the excited target residue with excitation energy distribution P(E*) and spin distribution P(J) would de-excite to the final reaction products by equilibrium particle emission. This equilibrium particle emission was simulated using the computer codes PACE[11] and LINDA.[12] In calculating the angular distribution of the final product nuclei with the LINDA code, all the pre-equilibrium (direct) particles were assumed to be emitted at an angle.

$$\theta = \frac{\hbar}{kR}$$

where R is the nuclear radius and k the nucleon wave number. This assumption (known as the Mantzouranis limit[13]) was made to be consistent with the calculations of the pre-equilibrium emission in the Blann model. Due to calculational difficulties in treating the high excitation energies involved in the 86 A MeV ^{12}C + ^{154}Sm reactions, we restricted our attention to the three systems with lower projectile energies.

4. Results

The individual target fragment yields for the reaction of heavy ions with ^{154}Sm are shown in Figure 1 while the isobaric yields derived from integrating the individual nuclidic yields while correcting for β-decay and unobserved species[14] are shown in Figure 2. In both figures, one can see the qualitative changes in reaction mechanism as the projectile energy increases. At the lowest energy (8.5 MeV/A), the fragment yield distribution is sharply peaked at a mass number near that of the completely fused system, with most of the reactions proceeding via a complete fusion mechanism. As the projectile energy increases, so does the energy deposited in the target nucleus, leading to the production (after deexcitation) of fragments of lower and lower mass numbers. Correspondingly, the fragment isobaric yield distribution becomes broader - but the decrease in the mass transfer from projectile to target nucleus causes the isobaric yield distribution to be asymmetric with a steeper upper edge and a long "spallation-like" tail towards lower masses. It is interesting to note that even at a projectile energy of 86 MeV/A, significant formation of trans-target species is observed although with somewhat less probability than in the reaction[3] of 86 MeV/A ^{2}C with ^{206}Pb, ^{209}Bi).

It is interesting to compare these data with the predictions of the Boltzmann master equation model discussed previously (Figure 3). The agreement between the measured isobaric yields and those predicted by the model is remarkably good, especially if one remembers the model has no adjustable parameters (as we used it). The agreement between calculation and data extends over a change in the yields of two orders of magnitude,

signifying a fundamentally correct simulation of the average behavior and the dispersion in that average.

Representative fragment angular distributions for the reactions of 19 MeV/A and 35 MeV/A projectiles with ^{154}Sm are shown in Figure 4. For the reactions induced by 19 MeV/A ^{16}O, ^{149}Gd and ^{151}Tb are typical "average" fragments while ^{155}Tb represents a trans-target product. Similarly ^{135}Ce and ^{145}Eu represent typical fragments for the reactions induced by 35 MeV/A ^{12}C. The angular distributions for the reactions involving 35 MeV/A ^{12}C projectiles are generally broader than those measured in reactions induced by 19 MeV/A ^{16}O due in part to the increased particle emission because of the larger energy deposit in the higher energy reaction. This can be shown by remembering that the mean square dispersion in the heavy fragment recoil angle, $\langle\theta_L\rangle$, due to particle emission is given by (15)

$$\bar{\theta}_L^2 \approx \frac{2}{3}\left(\frac{V}{v}\right)^2 \qquad (3)$$

if one assumes that particle emission is isotropic in the moving frame. V is the velocity of the recoil in the moving frame (due to kicks given it by particle emission) while v is the velocity of the moving frame (i.e., the velocity given the heavy product in the primary nuclear reaction to particle emission).

v can be taken as the mean projected fragment velocity as measured in the differential range experiments while V is given by (15)

$$V = \frac{\bar{\theta}_L \cdot v \cdot 4}{\pi} \qquad (4)$$

where $\bar{\theta}_L$ is the mean recoil angle. Use of equations (3) and (4) allows one to predict values of $\bar{\theta}_L^2$ of 0.022 rad^2 for ^{149}Gd and 0.0866 rad^2 for ^{135}Ce produced in the 19 MeV/A and 35 MeV/A reactions, respectively. These numbers are to be compared to the measured dispersions of 0.0267 rad^2 for ^{149}Gd and 0.119 rad^2 for ^{135}Ce. Thus it would seem that a major portion of the dispersion in the angular distributions is due to particle emission.

In Figure 4, we also compare the shape of the "average" target fragment angular distribution as predicted by the pre-equilibrium emission model to the data for typical "average" fragments. It appears that the calculated and measured angular distributions are in reasonably good agreement.

Another view of the changes in reaction mechanism with projectile energy can be obtained by examining a representative set of invariant velocity spectra. At the lowest projectile energy, (8.5 MeV/A ^{16}O), the velocity spectra show Gaussian peaks centered near the velocity of the completely fused system (Figure 5). If we take the number of events with $V > V_{CN}$ and double this number, assuming a Gaussian peak, we get a measure of the cross section for complete fusion (neglecting range straggling effects). For the interaction of 8.5 MeV/A ^{16}O with ^{154}Sm, 93% of the cross section is estimated to be associated with complete fusion reactions. Also, as seen in figure 4, the measured fragment velocity distribution for a typical fragment, ^{163}Tm, agrees well with the predictions of the Boltzmann master equation model.

For the reaction of 19 MeV/A ^{16}O with ^{154}Sm, the velocity spectrum of ^{151}Tb represents that of a typical product (Figure 5). The velocity

spectrum of ^{151}Tb can be thought of as a composite of spectra representing different reaction mechanisms, such as the spectra shown for ^{151}Gd (very incomplete fusion) and ^{156}Tb (near complete fusion). The average fragment velocity spectrum predicted by the Boltzmann master equation model is not in good agreement with the data. The problem seems to be that while the model predicts velocity spectra that have the correct shape and mean velocity for fusion-like processes (for example, production of ^{156}Tb), the model fails to predict the changes in the shape of the velocity spectra when incomplete fusion processes occur (such as the production of ^{151}Gd). It should be noted that the model <u>does</u> correctly predict the overall average fragment velocity for the reaction.

For the reaction of 35 MeV/A ^{12}C with ^{154}Sm, three typical fragment velocity spectra are shown (Figure 5). The nuclides involved represent different portions of the yield distribution for this reaction. All spectra show considerble amounts of incomplete fusion with mean fragment velocities being $\sim$ 1/2 that of the completely fused system. Because of the dominance of incomplete fusion processes in the velocity spectra of the representative fragments, the pre-equilibrium emission calculations do not yield velocity spectra with the correct shape although the mean fragment velocities are in agreement with the calculated results.

At 86 MeV/A, the velocity spectra of all typical products are dominated by incomplete fusion. The trans-target species ^{147}Eu shows the smallest velocities while the number of events with higher velocities (more "complete"

fusion, harder collisions) increases with decreasing fragment mass. Thus the production of trans-target species in the reaction of 86 MeV/A ^{12}C with heavy targets involves events with very small momentum (and energy) transfer allowing their survival even when produced in reactions involving moderately fissionable targets such as Pb and Bi.

The question may be posed as to why the pre-equilibrium calculations did such a good job of representing the fragment isobaric yields and their angular distributions and yet failed to give the correct shapes of the fragment velocity spectra at the higher projectile energies. A moment of reflection should suffice to provide a partial answer. For the three projectile energies at which the predictions of the pre-equilibrium model and the data have been compared, the number of pre-equilibrium nucleons that are emitted is modest (0.62, 2.98, 4.85 pre-equilibrium particles for projectile energies of 8.5, 19 and 35 A MeV, respectively). Consequently the isobaric yield distribution of the primary target residues following the pre-equilibrium nucleonic cascade is sharply peaked near the mass of the completely fused system. Similarly the angular distribution of the primary target residues is very strongly forward peaked along the beam direction. The shapes of the final (i.e., measured) product distributions are determined largely by the equilibrium de-excitation of the primary target residues and are, thus, not very sensitive to the details of the primary reaction mechanism, other than having the correct averge excitation energy and its distribution. (The latter point about having the correct distribution of the excitation energy is important since we did find that the use of a simple average excitation energy in the deexcitation calculations gave predictions that were in poor agreement with the isobaric yield distributions).

The velocity spectra are not very sensitive to the equilibrium de-excitation processes but are more sensitive to the primary reaction processes. The Boltzmann master equation model used in this work always predicts that the fragment velocity spectra have a symmetric Gaussian-like shape with the mean fragment velocity decreasing at the higher projectile energies. This shape is appropriate for central, fusion-like collisions where the pre-equilibrium cascade carries away significant fractions of the projectile momentum. However, the inclusive measured fragment velocity distributions are asymmetric in character with large numbers of low momentum transfer events (perhaps due to nucleon transfer, inelastic processes, etc.) along with other types of events not simulated in the pre-equilibrium calculations such as massive transfer or breakup fusion. Thus, the predicted and measured shapes of the velocity spectra differ. The remarkable feature of the pre-equilibrium calculations is that they do predict the "average" behavior so well, i.e., the average linear momentum transfer, the average fragment velocities, the average excitation energies and even the dispersion in excitation energy.

5. Summary and Conclusions

The data from this survey of processes producing target fragments in intermediate energy heavy ion reactions has shown the increasing importance of incomplete fusion processes leading to the asymmetric fragment isobaric yield and velocity distributions as the projectile energy increases. Production and survival of trans-target species occurs with significant probability at all projectile energies studied. The Boltzmann master equation model correctly predicts the average fractional linear momentum

transfer, the average target fragment velocities, angular and isobaric yield distributions. Differences between the shapes of the measured and predicted fragment velocity spectra can be understood in terms of processes not explicitly treated in the pre-equilibrium calculations (such as nucleon transfer, inelastic processes, massive transfer or breakup fusion).

Acknowledgements

This work was supported in part by the US Department of Energy under Contract DE-AC03-76SF00098 and De-AM06-76RLO2227, Task Agreement DE-AT06-76ER70035 Mod A007, the National Science Foundation and the Swedish Natural Science Research Council. We gratefully acknowledge the aid of the operations staff and health physics staff of the accelerators at LBL, MSU and CERN, Nuclear Data Inc. for loaning us equipment, Mr. P. Wilmarth of LBL and Mr. Jack Hernandez of Texas A & M for assistance in target preparation, and the members of the SHEIKS group for assistance in counting samples. Both KA and WDL wish to acknowledge the hospitality of the Lawrence Berkeley Laboratory during the time in which the experiments were performed and WDL wishes to further acknowledge the hospitality of the Studsvik Science Research Laboratory during preparation of a portion of this manuscript. We are deeply indebted to Marshall Blann for several stimulating discussions, and for furnishing us with a copy of the computer code used to make the pre-equilibrium calculations.

References

1. E. Tomasi, S. Leroy, C. Ngo, R. Lucas, D. Granier, C. Cerruti, P.L. Henoret, C. Mazer, M. Ribrag, J.L. Charvet, C. Humeau, J.P. Lochard, M. Morjean, Y. Patin, L. Sinopoli, J. Uzureau, A. DeMeyer, D. Guinet, L. Vagneron and A. Peghaire, Proc. Second Int'l Conf. on Nucleus-Nucleus Collisions, Vol I, p 60.

2. Loveland, W., Aleklett, K., McGaughey, P.L., Moody, K.J., McFarland, R.M., Kraus, R.H., Jr., and Seaborg, G.T., Phys. Rev. C. (submitted for publication).

3. Molzahn, D., Lund, T., Brandt, R., Hagebø, E., Haldorsen, I.R., and Serre, C.R., J. Radioanal. Chem. 80, (1983) 109.

4. Morrissey, D.J., Lee, D., Otto, R.J., and Seaborg, G.T., Nucl. Instr. Meth. 158, (1978) 499.

5. Kraus, Jr., R.H., Loveland, W., Aleklett, K., McGaughey, P.L., Sugihara, T.T., Seaborg, G.T., Lund, T., Morita, Y., Hagebø, E., and Haldorsen, I.R., Nucl. Phys. A432, (1985) 525.

6. Northcliffe, L.C., and Schilling, R.F., Nucl. Data Tables, 1, (1970) 233.

7. Winsberg, L., and Alexander, T., Phys. Rev. 121, 518 (1961).

8. M. Blann, Phys. Rev. C31, 1245 (1985).

9. M. Blann, Phys. Rev. C23, 205 (1981).

10. W.W. Wilke, J.R. Birkelund, H.J. Wollersheim, A.D. Hoover, J.R. Huizenga, W.U. Schroder and L.E. Tubbs, At. Data and Nucl. Data Tables 25 (1980).

11. A. Gavron, Phys. Rev. C21, 230 (1980).

12. E. Duek, L. Kowalski and J.M. Alexander, Comp. Phys. Comm. 34, 395 (1983)

13. G. Mantzourainis, H.A. Weidenmiller, and D. Agassi, Z. Phys. A276, 145 (1976).

14. Morrissey, D.J., Loveland, W., de Saint-Simon, M., and Seaborg, G.T., Phys. Rev. C21 (1980) 1783.

15. Alexander, J.M. in Nuclear Chemistry, Vol. I., Yaffe, L. Ed. (Academic Press, New York, 1968) p. 273.

Figure Captions

Figure 1. Plot of nuclidic yields for the reaction of a) 8.5 MeV/A and 19 MeV/A ^{16}O with ^{154}Sm and b) 35 MeV/A and 86 MeV/A ^{12}C with ^{154}Sm.

Figure 2. Fragment isobaric yield distributions for the reaction of various heavy ions with ^{154}Sm. The lines are to guide the eye through the data points.

Figure 3. Comparison of measured isobaric yield distributions with those predicted by the Boltzmann master equation model. The initial number of excitons in each case was taken to be $A_{proj} + 3$.

Figure 4. Representative laboratory system fragment angular distributions. The solid lines are to guide the eye while the dashed lines represent the predictions of the Boltzmann master equation model.

Figure 5. Representative velocity spectra for fragments from the reaction of intermediate energy heavy ions with ^{154}Sm. The dashed lines represent the predictions of the Boltzmann master equation model.

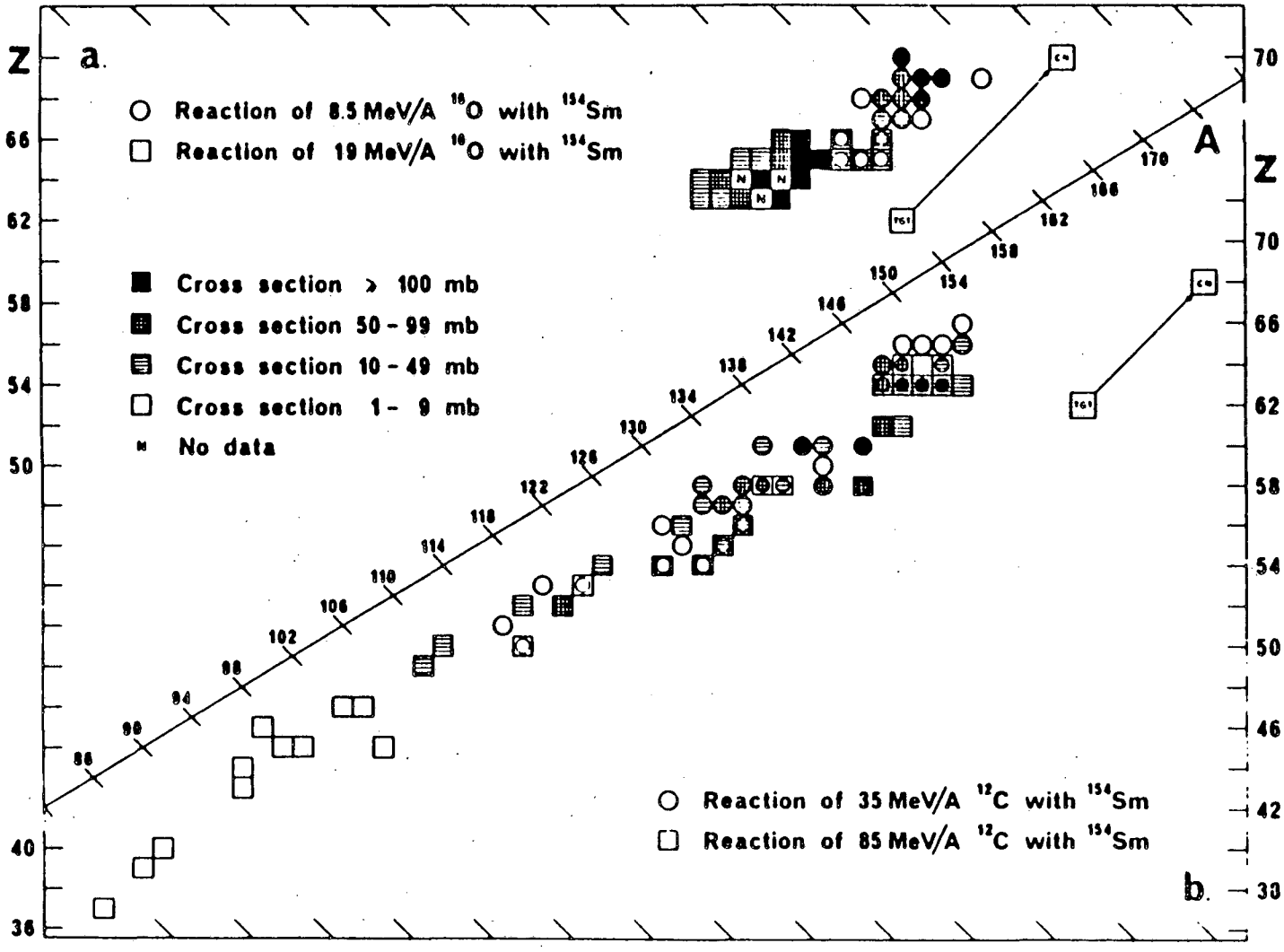
a.
Z
A
Reaction of 8.5 MeV/A ^{16}O with ^{154}Sm
Reaction of 19 MeV/A ^{16}O with ^{154}Sm
Cross section > 100 mb
Cross section 50 - 99 mb
Cross section 10 - 49 mb
Cross section 1 - 9 mb
No data
Reaction of 35 MeV/A ^{12}C with ^{154}Sm
Reaction of 85 MeV/A ^{12}C with ^{154}Sm
b.

Figure 1

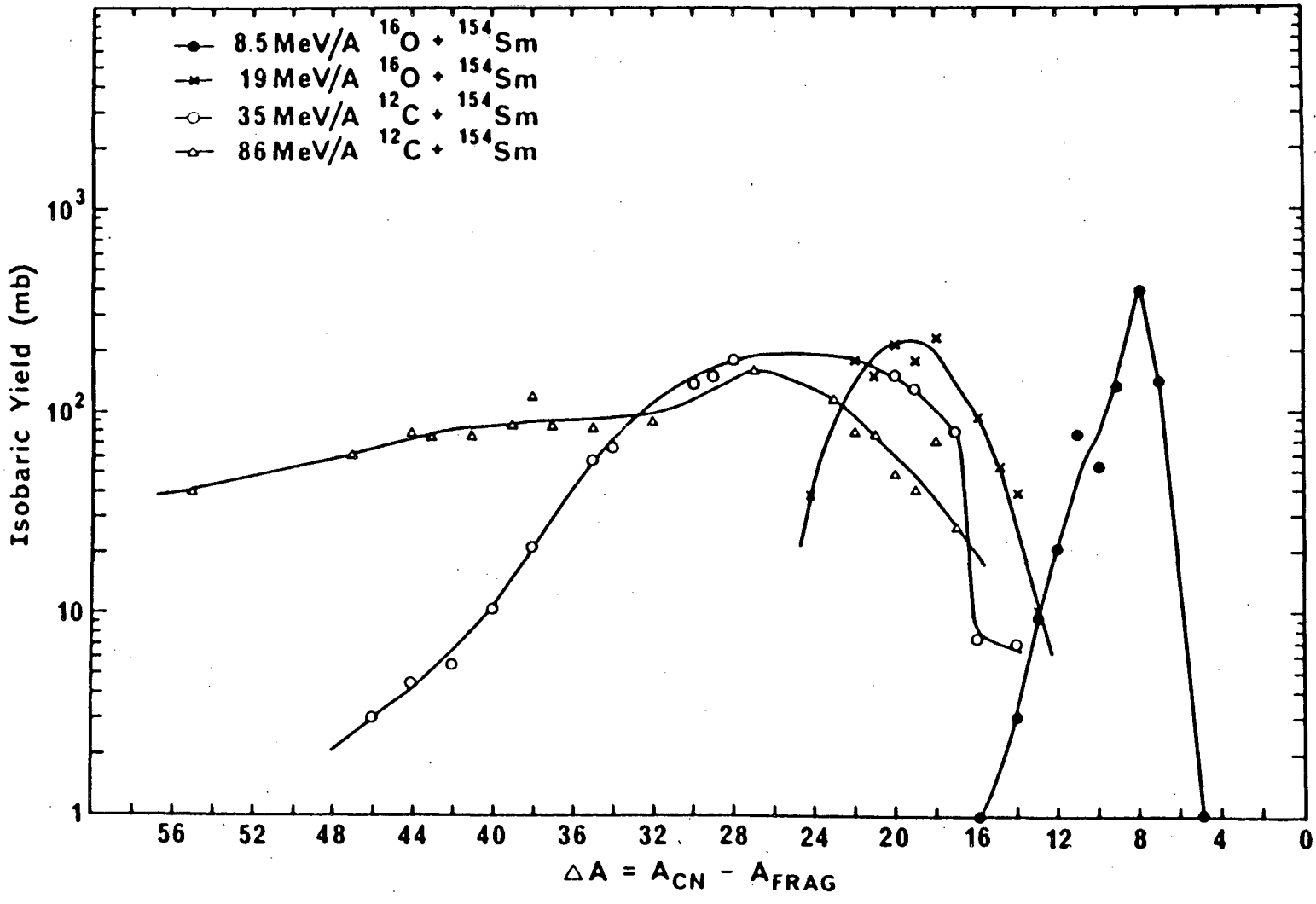
8.5 MeV/A ^{16}O + ^{154}Sm
19 MeV/A ^{16}O + ^{154}Sm
35 MeV/A ^{12}C + ^{154}Sm
86 MeV/A ^{12}C + ^{154}Sm
Isobaric Yield (mb)
10^3
10^2
10
1
56 52 48 44 40 36 32 28 24 20 16 12 8 4 0
$\Delta A = A_{CN} - A_{FRAG}$

Figure 2

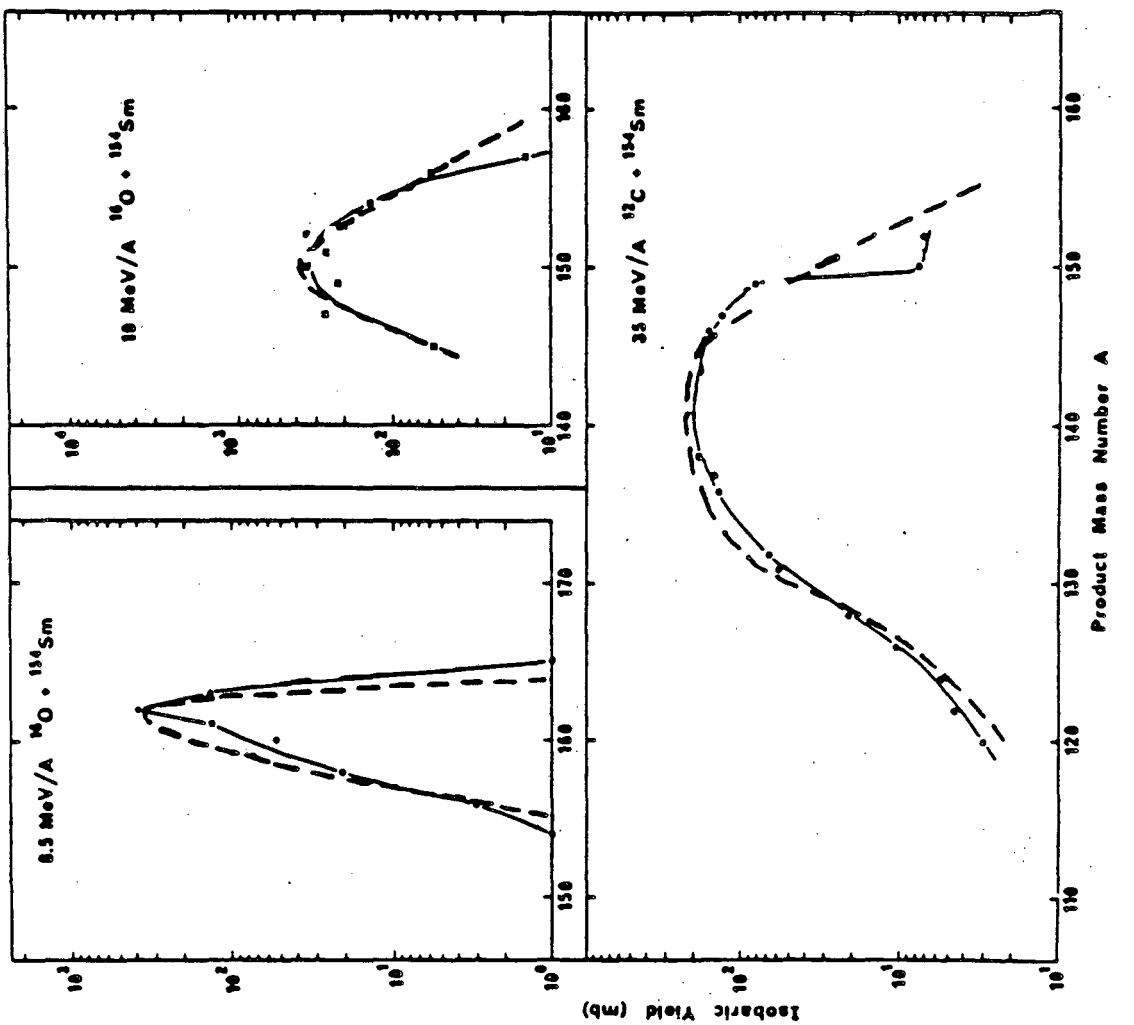
35 MeV/A ^{12}C + ^{154}Sm
18 MeV/A ^{16}O + ^{154}Sm
8.5 MeV/A ^{16}O + ^{154}Sm
Isobaric Yield (mb)
Product Mass Number A

Figure 3

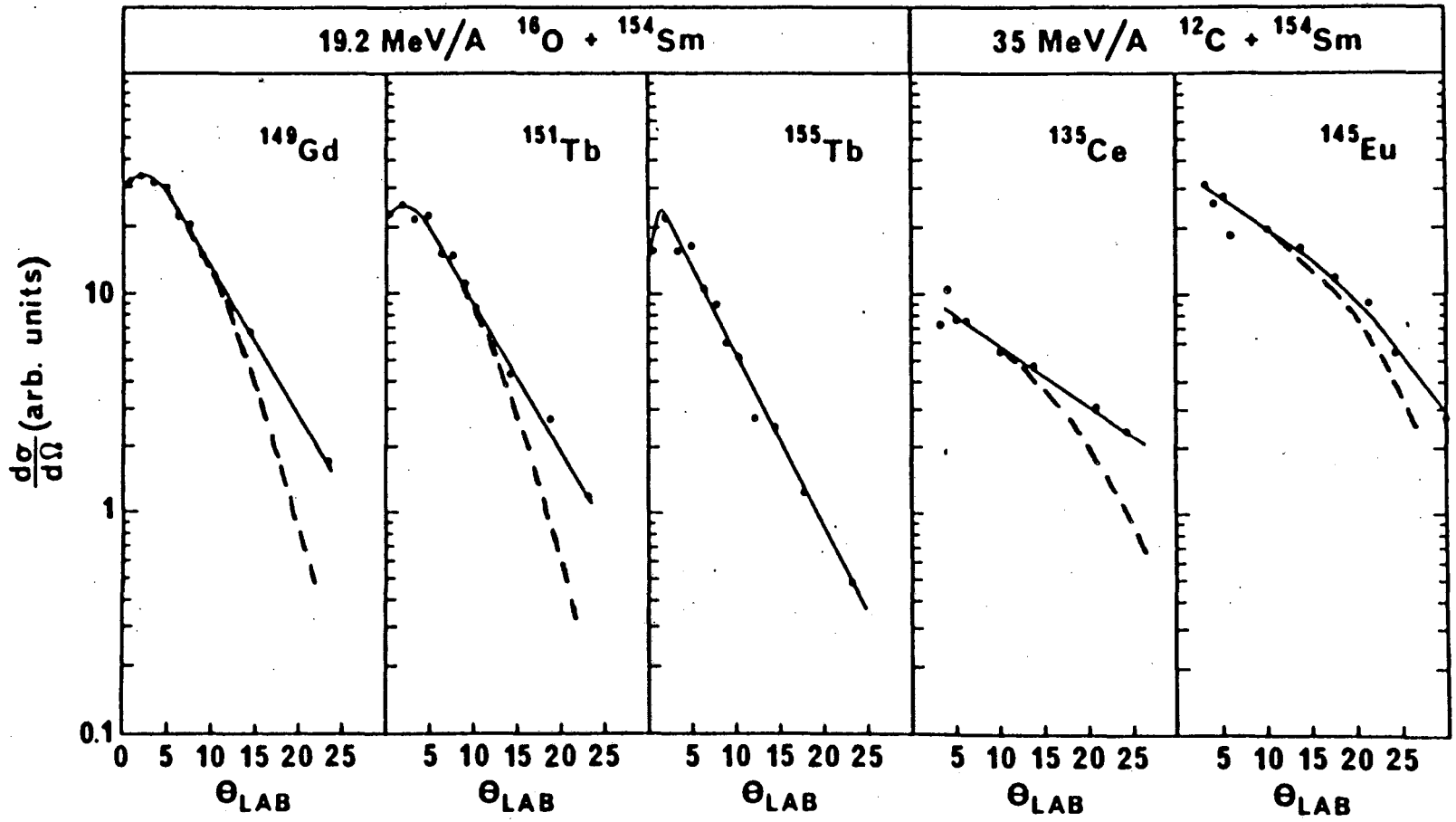
19.2 MeV/A ^{16}O + ^{154}Sm
35 MeV/A ^{12}C + ^{154}Sm
^{149}Gd
^{151}Tb
^{155}Tb
^{135}Ce
^{145}Eu
$\frac{d\sigma}{d\Omega}$(arb. units)
10
1
0.1
0 5 10 15 20 25
Θ_{LAB}

Figure 4

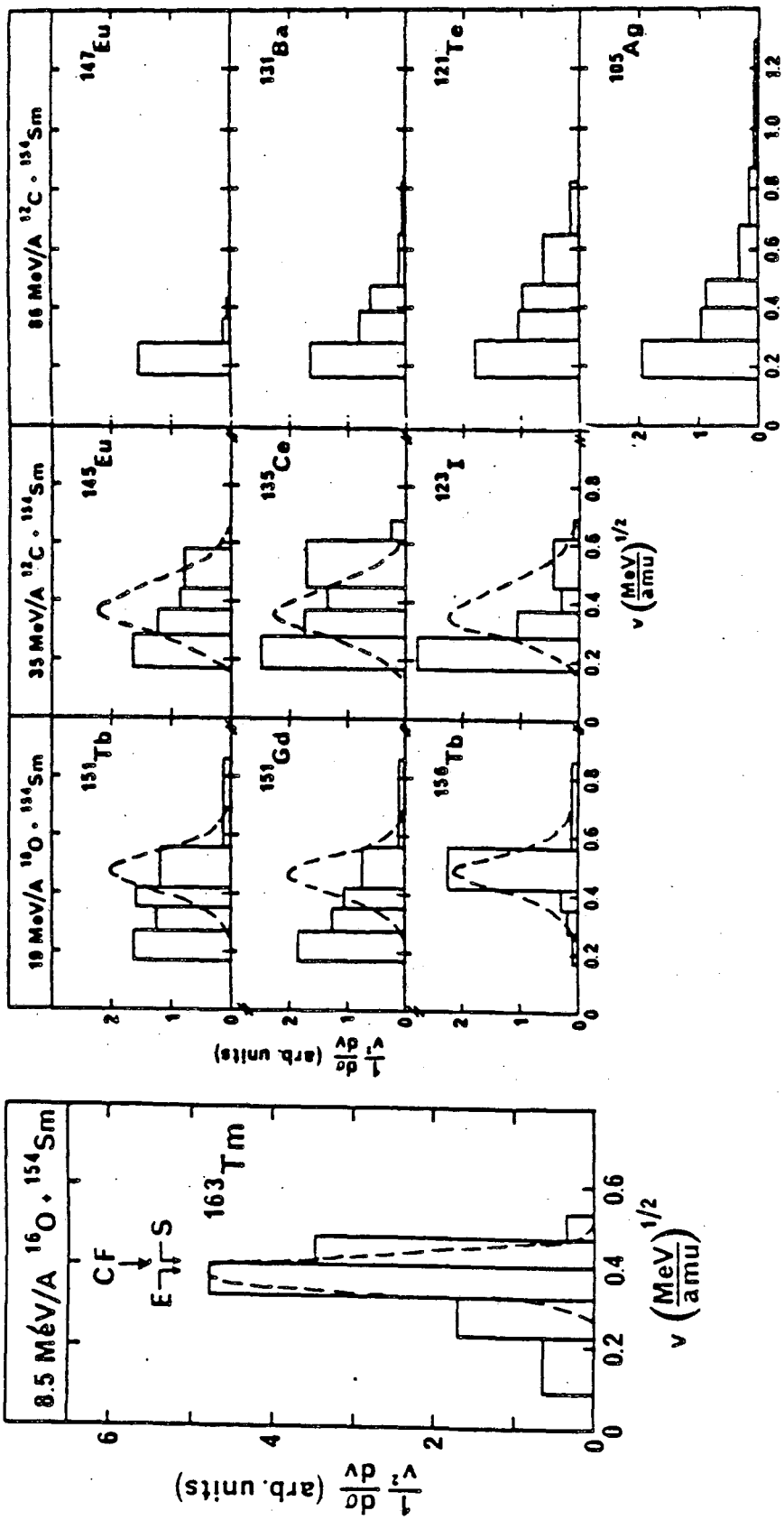
8.5 MeV/A ^{16}O + ^{154}Sm
^{163}Tm
CF
E
S
$\frac{1}{v^2}\frac{d\sigma}{dv}$ (arb. units)
$v\left(\frac{MeV}{amu}\right)^{1/2}$
10 MeV/A ^{16}O + ^{154}Sm
^{151}Tb
^{151}Gd
^{156}Tb
35 MeV/A ^{12}C + ^{154}Sm
^{145}Eu
^{135}Ce
^{123}I
88 MeV/A ^{12}C + ^{154}Sm
^{147}Eu
^{131}Ba
^{121}Te
^{105}Ag

Figure 5

LAWRENCE BERKELEY LABORATORY
TECHNICAL INFORMATION DEPARTMENT
UNIVERSITY OF CALIFORNIA
BERKELEY, CALIFORNIA 94720